

Plasmonic-Enhanced Polymer-Stabilized Liquid Crystals Switching for Integrated Optical Attenuation

Jialing Jian, Ruizhe Liu, Yuting Ye, Jianghong Wu, Qingyan Deng, Maoliang Wei, Yiheng Tang, Renjie Tang, Boshu Sun, Hui Ma, Yilin Shi, Chuyu Zhong, Chunlei Sun, Hongtao Lin, Ming Li,* and Lan Li*

Liquid crystals are widely used in photonics because of their profound electro–optic properties. However, the slow switching speeds (milliseconds) and the fluid nature of liquid crystals restrict their potential use in integrated photonics. In this work, polymer-stabilized liquid crystals are utilized as the functional material to improve the response time with a polymer network that helps pre-orientate the liquid crystal. Additionally, plasmonic slot structures are simultaneously employed to minimize the switch voltage by confining the optical field within the electrode spacing at subwavelength scales. Thanks to the large overlap of the optical and electric fields, the scattering states of the polymer-stabilized liquid crystal can be effectively manipulated to modulate the loss of the propagating wave, resulting in strong optical attenuation in the integrated photonic platform. Specifically, a plasmonic enhanced polymer-stabilized liquid crystal photonic device for operation at 1550 nm, which has a length of only 10 μm and shows an extinction ratio of 0.38 dB μm^{-1} , with a power consumption of less than 6 μW and a response time $\approx 20 \mu\text{s}$, resulting in a figure-of-merit of 0.012 mW.

in various optical devices, such as switches, phase shifters, modulators, and attenuators.^[6–9] By introducing LCs into integrated photonic platforms, on-chip dynamic modulation of light propagation can also be achieved with exceptional resolution and efficiency.^[10,11] However, current solutions are limited by slow switching speeds (in milliseconds), largely occupied working area (in millimeters), and the additional packaging and modulation burden caused by LCs' fluid nature, which restricts their large-scale and widespread applications.^[12–14]

To enhance the response speed and alleviate the impact of LCs' flow characteristics, polymer incorporation is used to form the polymer-stabilized liquid crystal (PSLC).^[15] The polymer network within the PSLC films plays a crucial role in the pre-alignment of LCs, facilitating the rapid restoration of the original optical states,

which can reduce response time by an order of magnitude down to 10^{-4} s (material system-dependent).^[16–18] PSLC films can also eliminate adverse effects such as liquid crystal backflow without additional energy consumption.^[19] Moreover, the modulation of light transmission of the PSLC film can be regulated to switch between a light-scattering and a transparent state by adjusting the electric field.^[20] Nevertheless, it is worth noting that

1. Introduction

Liquid crystals (LCs) are known for their high birefringence and ability to provide a large index contrast,^[1] which allows for significant light modulation and attenuation.^[2,3] They are also cost-effective and offer convenient and energy-efficient tunability^[4,5]

J. Jian
Zhejiang University
Hangzhou 310027, China

J. Jian, Y. Ye, J. Wu, Q. Deng, Y. Tang, R. Tang, B. Sun, Y. Shi, C. Sun, L. Li
Key Laboratory of 3D Micro/Nano Fabrication and Characterization of Zhejiang Province
School of Engineering
Westlake University
Hangzhou 310030, China
E-mail: lilan@westlake.edu.cn

J. Jian, Y. Ye, J. Wu, Q. Deng, Y. Tang, R. Tang, B. Sun, Y. Shi, C. Sun, L. Li
Institute of Advanced Technology
Westlake Institute for Advanced Study
18 Shilongshan Road, Hangzhou 310024, China

R. Liu, M. Wei, H. Ma, C. Zhong, H. Lin
State Key Laboratory of Brain-Machine Intelligence
College of Information Science and Electronic Engineering
Zhejiang University
Hangzhou 310027, China

M. Li
State Key Laboratory on Integrated Optoelectronics
Institute of Semiconductors
Chinese Academy of Sciences
Beijing 100083, China
E-mail: ml@semi.ac.cn

L. Li
Westlake Institute for Optoelectronics
Hangzhou 311421, China

 The ORCID identification number(s) for the author(s) of this article can be found under <https://doi.org/10.1002/adom.202400281>

DOI: 10.1002/adom.202400281

this PSLC strategy can lead to increased drive voltages, consequently lowering the modulation efficiency.^[21,22] One possible effective solution is to decrease the spacing between the electrodes to achieve smaller switching voltages^[3] while simultaneously enhancing the interaction between light and matter to improve the modulation efficiency and power consumption.^[23]

Plasmonic nanostructures have shown great potential in generating strong localized electric fields to enhance light-matter interaction on LC platforms. Previous research has focused on using metal nanoparticles^[24–26] or metallic metasurface structures^[27–29] to introduce plasmonic resonances. However, the use of metal nanoparticles introduces unpredictability in the material systems and limits tunability. Additionally, 2D metasurface structures present challenges regarding efficient optical coupling, working wavelength range, and electrode pad design for on-chip integrated modulation devices. Due to its compatibility with integrated photonic components, the plasmonic slot waveguide has gained significant attention as a potential solution for high-speed and efficient on-chip EO modulation.^[30–32] However, its application and verification in PSLCs have not yet been explored. Compact plasmonic slot waveguides can achieve the extreme confinement of light within a few micrometers,^[33] offering strong interaction between light and PSLC and a near-perfect overlap between optical and electronic signals across a broad optical wavelength range.^[34,35] Additionally, plasmonic slot waveguides feature extremely narrow electrode spacing (~100 nm). This characteristic allows for generating high electric field strength, decreasing the required drive voltage for optical modulation compared to silicon slot waveguides and reducing the device encapsulation and preparation burden.^[36]

In this study, we present a novel approach to utilizing plasmonic structures to enhance the electro-optic (EO) response of PSLC for on-chip integrated optical attenuation. Our device employs a plasmonic slot waveguide to capture optical field intensity change from the deflection of liquid crystals in PSLC film under electric field modulation, resulting in a compact modulator with an extinction ratio of 0.38 dB μm^{-1} . Meanwhile, this device surpasses the switching times of EO devices based on LCs, achieving speeds in the microsecond range while maintaining low power consumption at the microwatt level. The proposed device is equipped with a length of only 10 μm , a switching time of around 20 μs , and power consumption for one switching event as low as 6 μW , obtaining a significant improvement in figure of merit (FOM) (0.012 mW μs). All these results indicate the potential of plasmonic hybrid integrated devices for achieving ultra-compact and energy-efficient optical attenuation on a liquid crystal platform within microseconds.

2. Principle and Concept

Polymer/liquid crystal composite materials primarily utilize the birefringence of nematic liquid crystals (NLCs), which are reoriented under the action of an external field to make reversible transitions between ordered and disordered states, thus changing the overall transparency, as shown in **Figure 1a**. In the “ON” state, PSLCs are transparent, while in the “OFF” state, PSLCs become opaque due to the disorderly scattering of LC droplets in response to electric field modulation.^[37] In our device, the tran-

sition in PSLC films causes a change in the optical mode intensity at the telecom band.

In PSLC films, the dominant component is LCs, with a low mass fraction of polymers serving as stabilizers.^[38] We opted for NLCs (5CB) as they are well-suited for polymer/liquid crystal blends.^[39] Polycarbonate (PC) polymers are used to anchor the LCs in PSLC films,^[40,41] which construct the networks and establish the initial alignment of LCs while maintaining a specific orientational state without additional orientation procedures.^[16,42] This approach does not require extra energy consumption to maintain states, reduces preparation difficulty, and significantly decreases liquid crystals' response times.^[18,38,43] Depending on the material system, PSLC films based on 5CB LCs can reduce the response time from seconds to milliseconds.^[44–46]

However, introducing a polymer network can increase the drive voltage, reducing modulation efficiency. The driving performance (threshold voltage and saturation voltage) is closely related to electric field strength, which depends on the distance between the two electrodes.^[47] To suppress the drive voltage and increase the modulation efficiency, we employed a plasmonic slot waveguide (insert I of **Figure 1a**) to enhance the device performance. The plasmonic slot waveguide features the integration of two metal electrodes placed closely in a narrow spacing of ≈ 100 nm, providing an extremely strong electric field strength, as shown in **Figure 1b**. At the same time, the large permittivity contrast at metal surface-PSLC enables the compression of the optical mode field into the sub-wavelength range within the plasmonic slot waveguide (**Figure 1c**), thus effectively ensuring the considerable overlap of the optical and electrical fields within the slot region over a broad infrared wavelength range. The field-interaction factor (Γ) in a plasmonic slot waveguide approaches 1, at least three times larger than that in silicon slot waveguides.^[35,48] The strong localized effects of plasmonic structures guarantee that the on-chip fast and efficient modulation within a short (10 μm) PSLC film-integrated waveguide can be realized. In addition, the integration of this structure with PSLC reduces the electrical packaging burden on the LC-based materials and other photonic structures.

3. Results and Discussion

We investigated the EO properties of prepared PSLC films before evaluating the performance of the plasmonic-enhanced PSLC-integrated attenuation. The preparation process and parameters of the PSLC films can be found in Section S1.1 (Supporting Information). Due to the difficulty in characterizing the PSLC film within the plasmonic slot waveguide, PSLC films were coated onto metal electrodes with a spacing of 15 μm to simulate the variations of optical properties upon electrical field modulation. The proposed plasmonic-enhanced device has the same thickness of approximately 762 nm PSLC film as the prepared ones. To confirm the initial orienting effect of the polymer network on the LC, the reflection spectra of PSLC films were recorded using a microspectrophotometer (CRAIC 20/30PV) for linear polarized light at various angles. As depicted in **Figure 2a**, the film exhibited the strongest reflection at a polarization angle of 90° than other polarization angles. The consistent reflection spectra obtained from multiple positions highlight the considerable and systematic impact of the polymer network on the orientation of LCs.

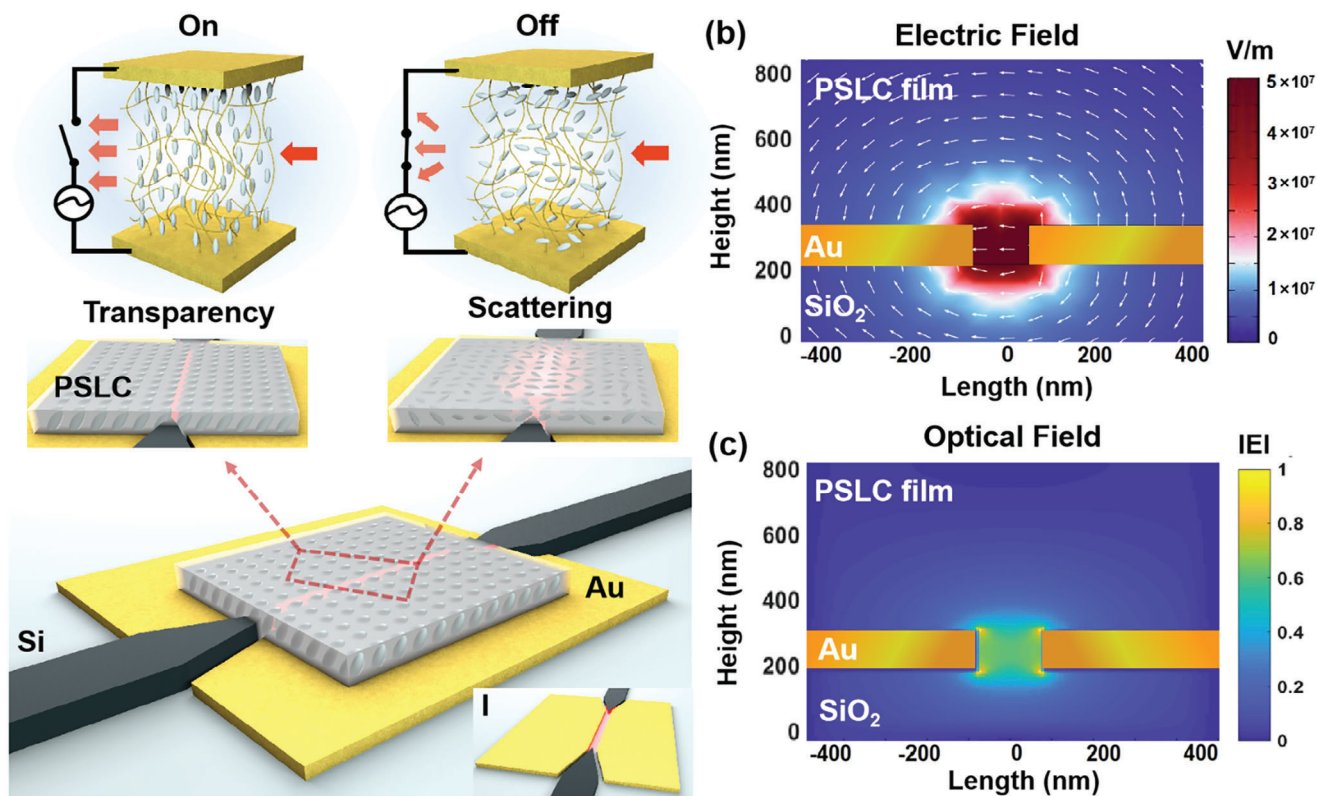


Figure 1. Device architecture and characteristics. a) Schematic diagram of the proposed device for plasmonic-enhanced polymer-stabilized liquid crystals switching for integrated optical attenuation, in which the plasmonic slot waveguide (Insert I) functions as an effective platform for guiding and manipulating light. Simulation results show the b) electric field strength of the plasmonic slot waveguide with the PSLC film at an applied voltage of 5 V and c) optical field of the TE mode in the plasmonic slot waveguide with the PSLC film without the applied voltage.

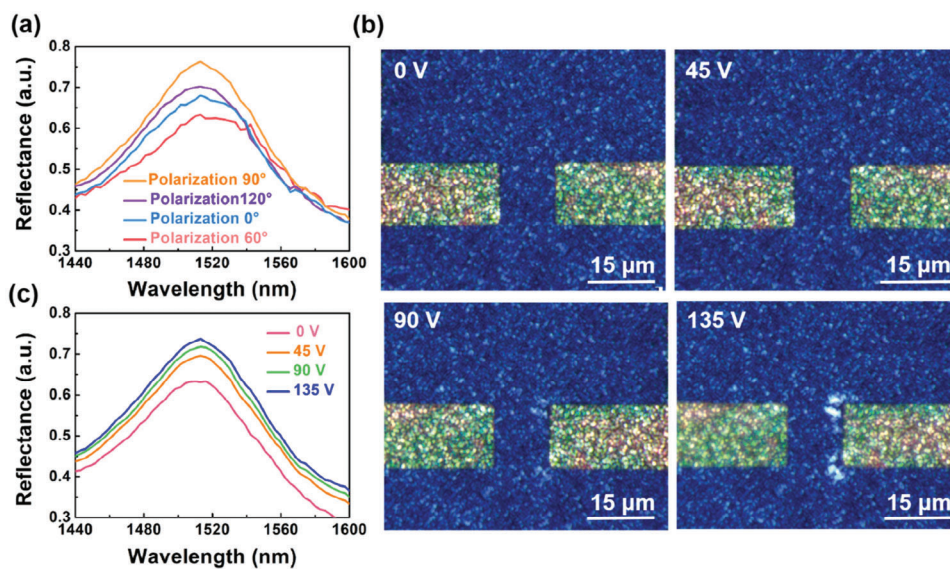


Figure 2. Characterization of PSLC films. a) Reflection spectra of PSLC films for incident light at different polarization angles (0° , 60° , 90° , 120°). b) Polarizing microscope images of the film at different applied voltages (0, 45, 90, 135 V). c) Microscale reflection spectra of the PSLC film recorded at different applied voltages (under linearly polarized light at 90°).

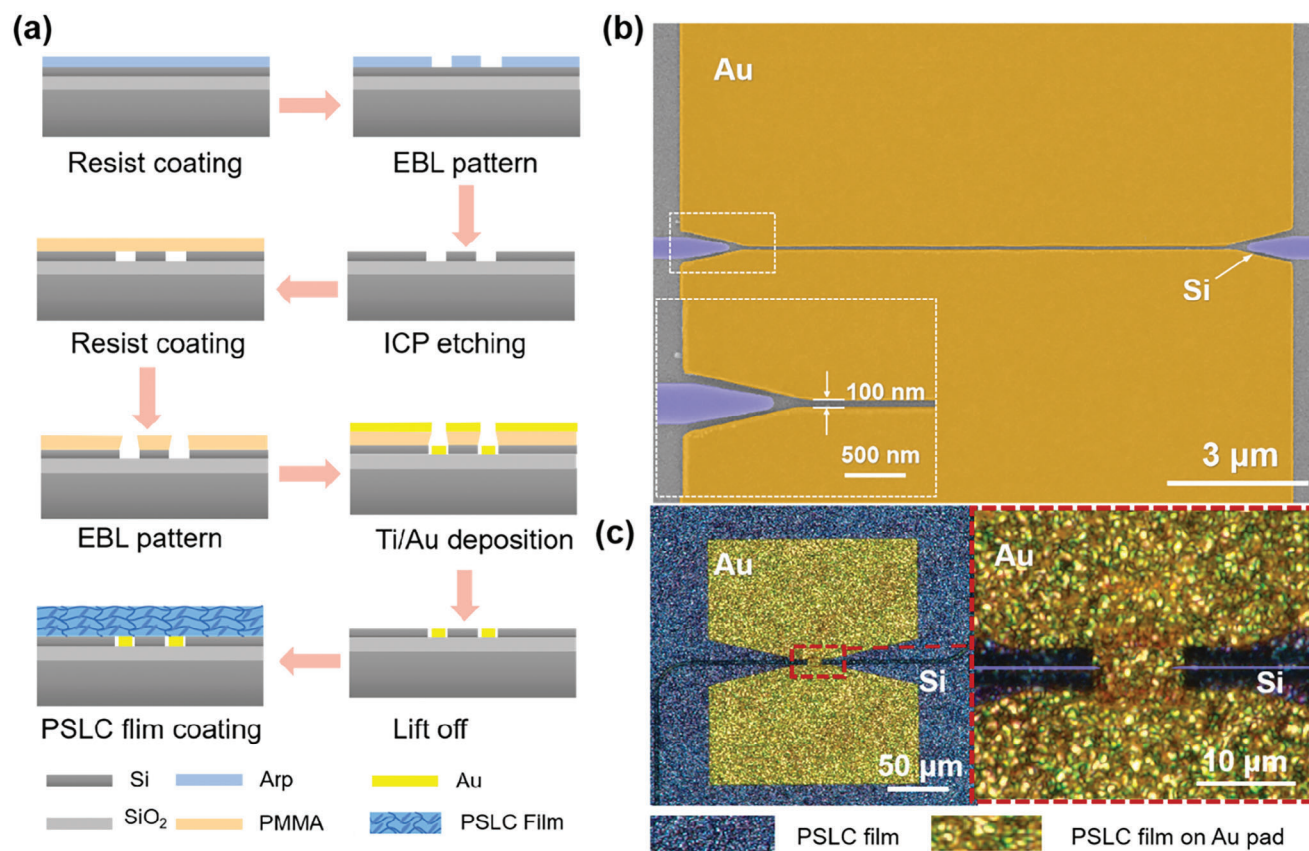


Figure 3. Characterization of the plasmonic-PSLC electronic-optic device. a) Schematic representation of the passive device fabrication process. b) SEM image of the plasmonic slot waveguide ($w_{\text{slot}} \times h_{\text{slot}} \approx 100 \times 100$ nm). c) Polarizing microscope images of the proposed device and its functional region.

Subsequently, we investigated the EO properties of the prepared PSLC films to confirm how the electric field modulates the optical state of the film at a polarization angle of 90° . As the applied electric field between the parallel electrodes increases, the PSLC experiences an accumulation of light scattering and changes in orientational state, indicated by the emergence of a progressively brighter white spot in Figure 2b. Meanwhile, the state switching is always observed at the tips of the electrode pads as the electric field strength is concentrated in those areas where the electric field intensity closely approximates that provided by the plasmonic slot waveguide, as shown in Section S2 (Supporting Information). It was noted that as the electric field strength increases, the scattering of light and disordering of orientations in the LC film is intensified, resulting in a higher optical loss in the PSLC films shown in Figure 2c. Drawing from these phenomena, we assert that using this film as cladding on a plasmonic slot waveguide, which can generate strong electric fields, offers a promising approach to manipulating the optical intensity of photonic devices.

We fabricated the proposed device to investigate plasmonic-enhanced optical attenuation performance in PSLC films. The preparation process is illustrated in Figure 3a, with specific details provided in Section S1.2 (Supporting Information). The device's active region comprises a pair of photonic-plasmonic mode converters (silicon-plasmonic tapered coupler) and a plasmonic

slot waveguide, as depicted in Figure 3b. The photonic mode in the silicon waveguide is converted into the plasmonic mode in the plasmonic slot waveguide by the silicon-plasmonic tapered coupler. The width (w_{slot}) and height (h_{slot}) of the plasmonic slot waveguide are denoted as $w_{\text{slot}} \times h_{\text{slot}}$ ($\approx 100 \times 100$ nm), with dimensions in the sub-micrometer range. This architectural configuration features an exceptionally narrow inter-electrode spacing providing ultrahigh electric field intensity (Figure 1b) and only supports the fundamental transverse electric (TE) mode (polarization 90°), as shown in Figure 1c. The proposed device, as illustrated in the insert of Figure 3c, includes two silicon coupling waveguides, a plasmonic slot waveguide, and the coated PSLC film on the top. The LC droplets are dispersed throughout the polymer network in PSLC film, with sizes on the sub-micrometer scale.^[49,50]

To further elucidate the operational principles of the device, we used an ellipsometer to extract refractive indices and absorption coefficients of the PSLC film (Figure S1e, Supporting Information) in the region near the electrode pads tips at various voltages, where the electric field intensity is more analogous to that in the plasmonic slot waveguide. Utilizing the obtained values, we integrated them into the plasmonic slot structure and simulated the optical field variations at different working voltages whose electric field intensity aligns with the region near the tips of the electrode pads. This involved estimating the effective refractive

Table 1. Effective refractive index, optical loss, and confinement factor of the TE mode in the device at different applied voltages.

Status	Applied voltage	Mode	n_{eff}	Loss [dB μm^{-1}]	Mode confinement factor [%]
Device without the PSLC film	0	TE	1.108	0.52	31.45
Device with the PSLC film	0	TE	1.528	2.03	20.40
Device with the PSLC film	0.75 V	TE	1.548	2.15	19.89
Device with the PSLC film	2.25 V	TE	1.673	3.41	15.41

indices, optical losses, and optical mode confinement factors for the optical TE modes. As shown in Table 1, increasing working voltage enhanced scattering within the PSLC films, leading to higher optical losses. Indeed, the disorder in LCs alignment driven by the voltage results in enhanced orientation disorder within the optical field, weakening the slot waveguide's confinement of light, as shown in Section S3 (Supporting Information). This conclusion is consistent with the observed variation pattern of the simulated optical mode confinement factor representing the ratio of light within the waveguide. To quantify the strength of the EO interaction of modulating field and optical mode, we calculated the field interaction factor Γ between PSLC and optical mode.^[51] The Γ is defined by Equation (1), traditionally used in the literature,^[52] and can also be approximated in a simplified form as

$$\Gamma \approx \frac{c\epsilon_0 n_{\text{mat}} \iint_{A_{\text{slot}}} |E_x(x, y)|^2 dx dy}{\iint_{-\infty}^{\infty} \text{Re}(E(x, y) \times H^*(x, y)) e_z dx dy} \quad (1)$$

where c is the speed of light, and n_{mat} represents the refractive index of active materials (PSLC). It is usually calculated as a ratio between the optical power in the cross-section of the interaction region and the total power propagating in the whole modal cross-section. In the case of plasmonic slot waveguides, Γ slightly underestimates $\Delta n_{\text{eff}}/\Delta n_{\text{mat}}$.^[35,52,53] In our device, the change in the effective refractive index of the device is 0.145, as shown in Table 1, and the refractive index of the material has varied by 0.16 under the influence of an electric field extracting from the ellipsometer. The calculated Γ is 0.91, nearly 2.8 times higher than existing reports based on silicon slot waveguides.^[54] Therefore, this demonstrates that the plasmonic slot waveguide imparts an ultrahigh responsiveness to the device for changes induced by the electric field in the PSLC film. Based on these findings, it is evident that the plasmonic slot architecture does help enhance the optical attenuation in the PSLC film-integrated photonic platform by providing ultrahigh electric field intensity and strong optical-electric field overlap.

Figure 4a depicts how the plasmonic-enhanced PSLC film-integrated device realizes the on-chip optical attenuation. When the PSLC film is transparent, the device is in the “on” state; when it scatters light, it is in the “off” state. We initially tested the device's optical losses under different voltages. As voltage rises, scattering intensifies, leading to increased optical losses. When a voltage below 2 V is applied to the device, there is little change

in optical loss. However, when the voltage exceeds 5 V, the device's loss tends to saturate. At a wavelength of 1550 nm, the extinction ratio using the extinction power per unit working area length^[55,56] can be calculated as 0.38 dB μm^{-1} at 5 V, demonstrating a strong modulation effect in Figure 4b. We checked that the switching voltage for the “off” state is at 1.89 V (90% to 10%), while the “on” state is at 4.15 V (10% to 90%). Additionally, the energy consumption (P) required for a single state transition is approaching 6 μW , as Figure 4c indicates. We cycled the device on/off five times with -5 and 5 V, as shown in Figure 4d. We tested it with 100 switching cycles, too. The measured 10–90% rise time (τ_{on}) is 28.87 μs , and the 90–10% (τ_{off}) fall time is 21.58 μs , primarily influenced by electrical driving intensity, as shown in Figure 4e,f. The plasmonic slot waveguide has greatly improved the device's response time compared to other integrated optical devices that use LCs or PSLCs as a basis with usually time constants of milliseconds.^[44,57] To compare the performance of the optical devices with those of previously reported works, the FOM was defined as $P \cdot \tau$ (mW μs). Here, P is the electric power for achieving a single state transition, and τ is the average value of the response time constant τ_{on} and τ_{off} . The FOM of 0.012 mW μs was achieved, which at least reduces three orders of magnitude than other EO switches, as shown in Table S1 (Supporting Information).

We also examined the dynamic response of plasmonic-enhanced PSLC devices at various temperatures. This investigation was important because the devices' response time can be affected by the LCs' viscoelastic properties, which are highly dependent on temperature.^[47] Figure 5a shows the experimental configuration for device testing, wherein a temperature control system was used to adjust the environmental temperature. We applied the signals with the same intensity and frequency to measure the device's response time at various temperatures. First, as shown in Figure 5b, the contrast between the “ON” and “OFF” states decreases. This phenomenon is due to the transition of the behavior of LCs from anisotropic to isotropic as the temperature approaches the clearing point (55–60 °C) and the refractive index of the LCs approaches the unusual refractive index (n_o), resulting in the temporary disappearance of the scattering state in the film.^[58] In addition, as the temperature increases, we observe that τ_{off} of the device decreases while τ_{on} increases, as shown in Figure 5b. Theoretically, the response time can be predicted according to Equations (2) and (3)

$$\tau_{\text{on}} \approx \frac{\sigma}{\Delta\epsilon V^2 - \frac{K(l^2-1)}{R^2}} \quad (2)$$

$$\tau_{\text{off}} \approx \frac{R^2 \sigma}{K(l^2 - 1)} \quad (3)$$

where V is the applied electric field, the droplet radius (R) of LCs, while other parameters are related to polymer /LC blends, including elastic constant (K), dielectric anisotropy ($\Delta\epsilon$), shape anisotropy (l), and rotational viscosity constant (σ), respectively.^[59–61] With the temperature rise, the shape anisotropy (l) and dielectric anisotropy ($\Delta\epsilon$) of the LC molecules decrease, leading to an increase in τ_{on} according to Equation (2).^[16] Based on Equation (3), the rotational viscosity constant (σ) of LC molecules may decrease as the temperature

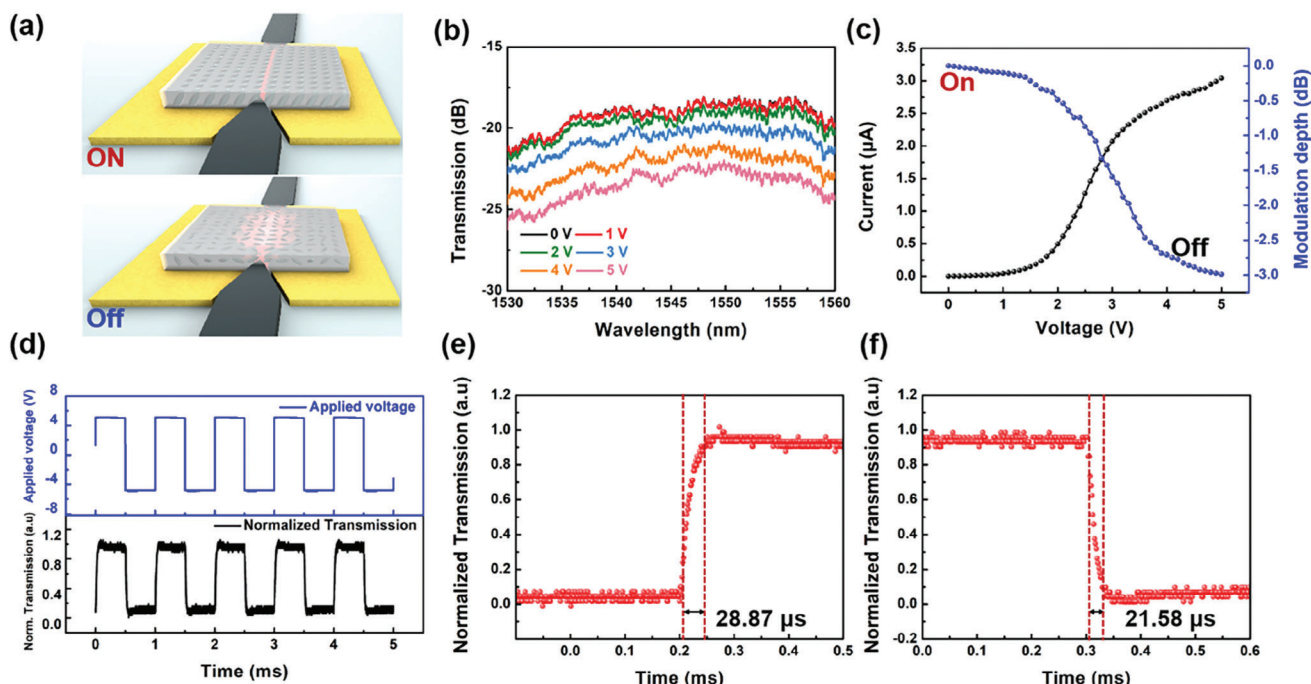


Figure 4. Electronic–optic response of the proposed device at 25 °C. a) Schematic illustration of the device film status in on and off states. b) Comparison of optical losses in the device at different applied voltages. c) Current and optical power variation at different applied voltages. d) Real-time trace of the device's normalized optical transmission (black line) with the corresponding applied voltage (blue line) during five switching on and off cycles. Measured temporal responses of e) on and f) off states in the device.

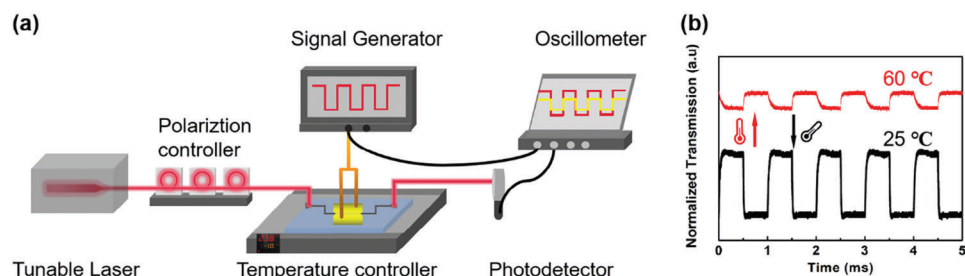


Figure 5. Dynamic response testing of the device at different temperatures. a) Schematic diagram of the device testing setup at different temperatures. b) Real-time variations of the device's dynamic response measured at different temperatures, including both before and after the clearing point temperature of the liquid crystal.

increases, lowering the rotational resistance of the LC molecules, which leads to a decrease in τ_{off} .^[47] Consequently, with temperature changes, the difference between the rising and falling edges of the response becomes more pronounced. As shown in Table 2, the device's switching speed remains around 20 μs , indicating that our device's switching time can consistently stay within this range, suggesting that the effect of the plasmonic structure on the performance enhancement of the proposed device is very stable.

As a result, it can be seen that the proposed design offers a novel approach to developing power-efficient LC-integrated de-

vices that can potentially achieve single-digit microsecond responses and intensity modulation across a wide temperature range. This highlights a significant advantage of LC-based devices compared to others,^[57] as detailed in Table S1 (Supporting Information). In our subsequent work, we can improve the device performance by choosing LCs with higher clearing points,^[62] optimizing the LC-to-polymer ratio.^[63] Additionally, we can further enhance the modulation efficiency by doping nanoparticles into the PSLC films, thus improving the refractive index contrast of the thin film and suppressing the threshold voltage.

Table 2. Device switching states and response times at different temperatures.

Temperature [°C]	25	30	35	40	45	50	55	60
Response time [μs]	21.58	21.53	18.03	15.53	12.67	12.49	11.60	28.61

4. Conclusion

In this study, we utilized a plasmonic slot waveguide to enhance the EO properties of PSLC to offer an energy-efficient, fast, and compact solution for integrated optical attenuation.

Polymer-stabilized liquid crystals serve as one kind of reconfigurable material in photonic switch devices, enabling sub-millisecond response times through electronic control of material scattering. The introduction of polymer enhances the response speed of liquid crystal and mitigates the negative effects of liquid crystal flow on the fabrication process. Plasmonic slot waveguides accomplish a perfect overlap between the optical and electrical fields, providing not only an ultra-narrow electrode spacing to reduce switch voltages but also a robust optical field confinement to enhance the device's modulation efficiency, resulting in an extinction ratio of 0.38 dB μm^{-1} . The device is only 10 μm in length, with estimated power consumption below 6 μW , and a response time of approximately 20 μs , corresponding to a FOM of 0.012 mW μs . This expands the applications of liquid crystal devices in integrated photonics, offering a viable solution for achieving low-power consumption, high-speed, and ultracompact optical switches and attenuators.

5. Experimental Section

Experimental details, including materials, characterizations, simulation, and measurement, are listed in the Section S1 (Supporting Information).

Supporting Information

Supporting Information is available from the Wiley Online Library or from the author.

Acknowledgements

The authors thank the Westlake Center for Micro/Nano Fabrication, Instrumentation and Service Center for Physical Sciences at Westlake University, and ZJU Micro-Nano Fabrication Center at Zhejiang University for the facility support. The authors thank Dr. Zhong CHEN from the Instrumentation and Service Center for Molecular Sciences at Westlake University for support in Raman measurement. This work was primarily supported by the Zhejiang Provincial Natural Science Foundation of China (LD22F040002); National Natural Science Foundation of China (12104375, 62175202, and 92150302); Special Support Plan for Photoelectric Chips Research at Westlake University (10300000H062401/001); the Key Project of Westlake Institute for Optoelectronics (2023GD003/110500Y0022303).

Conflict of Interest

The authors declare no conflict of interest.

Data Availability Statement

The data that support the findings of this study are available from the corresponding author upon reasonable request.

Keywords

plasmonic integrated device, plasmonic slot waveguide, polymer-stabilized liquid crystal

Received: January 30, 2024

Revised: March 13, 2024

Published online:

- [1] P. Kirsch, M. Bremer, *Angew. Chem., Int. Ed.* **2000**, *39*, 4216.
- [2] K. Yin, E. L. Hsiang, J. Zou, Y. Li, Z. Yang, Q. Yang, P. C. Lai, C. L. Lin, S. T. Wu, *Light Sci. Appl.* **2022**, *11*, 161.
- [3] R. Zhang, Z. Zhang, J. Han, L. Yang, J. Li, Z. Song, T. Wang, J. Zhu, *Light Sci. Appl.* **2023**, *12*, 11.
- [4] U. S. Tripathi, A. Bijalwan, V. Rastogi, *IEEE Photonic. Tech. L* **2020**, *32*, 1453.
- [5] L. Y. Chiang, C. T. Wang, T. S. Lin, S. Pappert, P. Yu, *Opt. Express* **2020**, *28*, 29345.
- [6] L. A. Joerg Pfeifle, W. Freude, J. Leuthold, C. Koos, *Opt. Express* **2012**, *20*, 18.
- [7] G. Zhu, B. Wei, L. Shi, X. Lin, W. Hu, Z. Huang, Y. Lu, *Opt. Express* **2013**, *21*, 5332.
- [8] L. Van Iseghem, E. Picavet, A. Y. Takabayashi, P. Edinger, U. Khan, P. Verheyen, N. Quack, K. B. Gylfason, K. De Buysser, J. Beeckman, W. Bogaerts, *Opt. Mater. Express* **2022**, *12*, 2181.
- [9] A. Kato, K. Nakatsuhara, Y. Hayama, *J. Light. Technol.* **2014**, *32*, 4464.
- [10] L. Chiang, C. Wang, S. Pappert, P. K. L. Yu, *IEEE Photonic. Tech. L* **2021**, *33*, 796.
- [11] Y. Shin, Y. Jiang, Q. Wang, Z. Zhou, G. Qin, D. Yang, *Photon. Res.* **2022**, *10*, 407.
- [12] M. Notaros, T. Dyer, M. Raval, C. Baiocco, J. Notaros, M. R. Watts, *Opt. Express* **2022**, *30*, 13790.
- [13] L. Y. Chiang, C. T. Wang, S. Pappert, P. K. L. Yu, presented at *2021 5th IEEE Electron Devices Technology & Manufacturing Conf. (EDTM)*, Chengdu, China, April, **2021**.
- [14] Y. Atsumi, K. Watabe, N. Uda, N. Miura, Y. Sakakibara, *Opt. Express* **2019**, *27*, 8756.
- [15] Y. Li, Z. Yang, R. Chen, L. Mo, J. Li, M. Hu, S. T. Wu, *Polymers* **2020**, *12*, 2862.
- [16] H. Kikuchi, M. Yokota, Y. Hisakado, H. Yang, T. Kajiyama, *Nat. Mater.* **2002**, *1*, 64.
- [17] J. Heo, J. Huh, T. Yoon, *AIP Adv.* **2015**, *5*, 047118.
- [18] H. Fujikake, T. Kuki, T. Nomoto, Y. Tsuchiya, Y. Utsumi, *J. Appl. Phys.* **2001**, *89*, 5295.
- [19] J. Wu, Y. Ye, J. Jian, X. Yao, J. Li, B. Tang, H. Ma, M. Wei, W. Li, H. Lin, L. Li, *Nano Lett.* **2023**, *23*, 6440.
- [20] C. Yun, M. H. Saeed, D. Kim, K. Kim, M. Choi, S. Park, J. Na, *ACS Appl. Polym. Mater.* **2023**, *5*, 3919.
- [21] C. Li, M. Chen, L. Zhang, W. Shen, X. Liang, X. Wang, H. Yang, *Liq. Cryst.* **2019**, *47*, 106.
- [22] J. Chen, C. Li, L. Sun, L. Ma, B. Li, Y. Lu, *Chin. Opt. Lett.* **2022**, *20*, 023201.
- [23] J. Wu, H. Ma, P. Yin, Y. Ge, Y. Zhang, L. Li, H. Zhang, H. Lin, *Small Sci.* **2021**, *1*, 2000053.
- [24] Y.-S. Ha, H.-J. Kim, H.-G. Park, D.-S. Seo, *Opt. Express* **2012**, *20*, 6448.
- [25] S. Khatua, P. Manna, W.-S. Chang, A. Tcherniak, E. Friedlander, E. R. Zubarev, S. Link, *J. Phys. Chem. C* **2010**, *114*, 7251.
- [26] G. Lee, G. Park, J. G. Park, Y. Bak, C. Lee, D. K. Yoon, *Adv. Mater.* **2024**, *36*, 2307388.
- [27] F. Petronella, T. Madeleine, V. De Mei, F. Zaccagnini, M. Striccoli, G. D'Alessandro, M. Rumi, J. Slagle, M. Kaczmarek, L. De Sio, *ACS Appl. Mater. Interfaces* **2023**, *15*, 49468.
- [28] M. Sharma, L. Michaeli, D. B. Haim, T. Ellenbogen, *ACS Photonics* **2022**, *9*, 2702.
- [29] H. Yu, M. Jiang, Y. Guo, T. Turiv, W. Lu, V. Ray, O. D. Lavrentovich, Q.-H. Wei, *Adv. Opt. Mater.* **2019**, *7*, 1900117.
- [30] M. Burla, C. Hoessbacher, W. Heni, C. Haffner, Y. Fedoryshyn, D. Werner, T. Watanabe, H. Massler, D. L. Elder, L. R. Dalton, J. Leuthold, *APL Photonics* **2019**, *4*, 056106.
- [31] U. Koch, C. Uhl, H. Hettrich, Y. Fedoryshyn, C. Hoessbacher, W. Heni, B. Baeuerle, B. I. Bitachon, A. Josten, M. Ayata, H. Xu, D. L. Elder, L. R. Dalton, E. Mentovich, P. Bakopoulos, S. Lischke, A. Krüger, L.

- Zimmermann, D. Tsiokos, N. Pleros, M. Möller, J. Leuthold, *Nat. Electron.* **2020**, *3*, 338.
- [32] Y. Horst, B. I. Bitachon, L. Kulmer, J. Brun, T. Blatter, J. M. Conan, A. Montmerle-Bonnefois, J. Montri, B. Sorrente, C. B. Lim, N. Vedrenne, D. Matter, L. Pommarel, B. Baeuerle, J. Leuthold, *Light. Sci. Appl.* **2023**, *12*, 153.
- [33] C. Haffner, D. Chelladurai, Y. Fedoryshyn, A. Josten, B. Baeuerle, W. Heni, T. Watanabe, T. Cui, B. Cheng, S. Saha, D. L. Elder, L. R. Dalton, A. Boltasseva, V. M. Shalaev, N. Kinsey, J. Leuthold, *Nature* **2018**, *556*, 483.
- [34] D. K. Gramotnev, S. I. Bozhevolnyi, *Nat. Photonics* **2010**, *4*, 83.
- [35] C. Haffner, W. Heni, Y. Fedoryshyn, J. Niegemann, A. Melikyan, D. L. Elder, B. Baeuerle, Y. Salamin, A. Josten, U. Koch, C. Hoessbacher, F. Ducry, L. Juchli, A. Emboras, D. Hillerkuss, M. Kohl, L. R. Dalton, C. Hafner, J. Leuthold, *Nat. Photonics* **2015**, *9*, 525.
- [36] W. Heni, C. Haffner, D. L. Elder, A. F. Tillack, Y. Fedoryshyn, R. Cottier, Y. Salamin, C. Hoessbacher, U. Koch, B. Cheng, B. Robinson, L. R. Dalton, J. Leuthold, *Opt. Express* **2017**, *25*, 2627.
- [37] M. H. Saeed, S. Zhang, Y. Cao, L. Zhou, J. Hu, I. Muhammad, J. Xiao, L. Zhang, H. Yang, *Molecules* **2020**, *25*, 5510.
- [38] A. Gruzdenko, I. Dierking, *J. Mater. Chem. C* **2023**, *11*, 5438.
- [39] G. Chen, M. Ni, H. Peng, F. Huang, Y. Liao, M. Wang, J. Zhu, V. A. Roy, X. Xie, *ACS Appl. Mater. Interfaces* **2017**, *9*, 1810.
- [40] W. H. Jo, H. Yim, I. Kwon, T. Son, *Polym. J.* **1992**, *24*, 519.
- [41] G. Tovar, P. J. Carreau, H. P. Schreiber, *Colloids. Surf. A* **2000**, *161*, 213.
- [42] J. B. Wu, S. B. Wu, H. M. Cao, Q. M. Chen, Y. Q. Lu, W. Hu, *Adv. Opt. Mater.* **2022**, *10*, 2201015.
- [43] J. L. Zhu, S. B. Ni, Y. Song, E. W. Zhong, Y. J. Wang, C. Ping Chen, Z. Ye, G. He, D. Q. Wu, X. L. Song, J. G. Lu, Y. Su, *Appl. Phys. Lett.* **2013**, *102*, 071104.
- [44] H. C. Lin, Y. H. Lin, *Appl. Phys. Lett.* **2011**, *98*, 083503.
- [45] M. Khan, S. Y. Park, *Anal. Chem.* **2014**, *86*, 1493.
- [46] G. Sinha, J. Leys, C. Glorieux, J. Thoen, *Phys. Rev. E* **2005**, *72*, 051710.
- [47] K. Amundson, *Phys. Rev. E* **1996**, *53*, 2412.
- [48] M. Laueremann, R. Palmer, S. Koeber, P. C. Schindler, D. Korn, T. Wahlbrink, J. Bolten, M. Waldow, D. L. Elder, L. R. Dalton, J. Leuthold, W. Freude, C. Koos, *Opt. Express* **2014**, *22*, 29927.
- [49] A. Parshin, V. Gulyakov, V. Zyryanov, V. Shabanov, *Int. J. Mol. Sci.* **2013**, *14*, 16303.
- [50] Q. Lin, J. Jho, A. F. Yee, *Polym. Eng. Sci.* **2004**, *33*, 789.
- [51] G. W. Lu, J. Hong, F. Qiu, A. M. Spring, T. Kashino, J. Oshima, M. A. Ozawa, H. Nawata, S. Yokoyama, *Nat. Commun.* **2020**, *11*, 4224.
- [52] J. M. Brosi, C. Koos, L. C. Andreani, M. Waldow, J. Leuthold, W. Freude, *Opt. Express* **2008**, *16*, 4177.
- [53] J. Witzens, T. Baehr-Jones, M. Hochberg, *Opt. Express* **2010**, *18*, 16902.
- [54] J. Ronn, W. Zhang, A. Autere, X. Leroux, L. Pakarinen, C. A. Ramos, A. Saynatjoki, H. Lipsanen, L. Vivien, E. Cassan, Z. Sun, *Nat. Commun.* **2019**, *10*, 432.
- [55] Y. Ding, X. Zhu, S. Xiao, H. Hu, L. H. Frandsen, N. A. Mortensen, K. Yvind, *Nano Lett.* **2015**, *15*, 4393.
- [56] S. Zhu, Y. Liu, L. Shi, X. Xu, X. Zhang, *Photon. Res.* **2016**, *4*, 191.
- [57] Y. Xing, T. Ako, J. P. George, D. Korn, H. Yu, P. Verheyen, M. Pantouvaki, G. Lepage, P. Absil, A. Ruocco, C. Koos, J. Leuthold, K. Neyts, J. Beeckman, W. Bogaerts, *IEEE Photonic. Tech. L* **2015**, *27*, 1269.
- [58] M. Mucha, *Prog. Polym. Sci.* **2003**, *28*, 837.
- [59] P. S. Drzaic, *Liq. Cryst.* **1988**, *3*, 1543.
- [60] F. P. Nicoletta, G. d. Filpo, I. Bellini, G. Chidichimo, *Mol. Cryst. Liq. Cryst.* **1999**, *336*, 93.
- [61] B. Wu, J. H. Erdmann, J. W. Doane, *Liq. Cryst.* **1989**, *5*, 1453.
- [62] P. Malik, S. Yadav, Khushboo, *J. Mol. Struct.* **2019**, *1188*, 51.
- [63] W. Shen, G. Li, *Laser. Photonics. Rev.* **2022**, *17*, 2200207.